

MOIRAI-MOE: EMPOWERING TIME SERIES FOUNDATION MODELS WITH SPARSE MIXTURE OF EXPERTS

Xu Liu^{1,2*}, Juncheng Liu¹, Gerald Woo^{1*}, Taha Aksu¹, Yuxuan Liang³, Roger Zimmermann², Chenghao Liu^{1†}, Silvio Savarese¹, Caiming Xiong¹, Doyen Sahoo¹

¹Salesforce AI Research, ²National University of Singapore,

³The Hong Kong University of Science and Technology (Guangzhou)

ABSTRACT

Time series foundation models have demonstrated impressive performance as zero-shot forecasters, i.e., they can tackle a wide variety of downstream forecasting tasks without explicit task-specific training. However, achieving effectively unified training on time series remains an open challenge. Existing approaches introduce some level of model specialization to account for the highly heterogeneous nature of time series data. For instance, MOIRAI pursues unified training by employing multiple input/output projection layers, each tailored to handle time series at a specific frequency. Similarly, TimesFM maintains a frequency embedding dictionary for this purpose. We identify two major drawbacks to this human-imposed frequency-level model specialization: (1) Frequency is not a reliable indicator of the underlying patterns in time series. For example, time series with different frequencies can display similar patterns, while those with the same frequency may exhibit varied patterns. (2) Non-stationarity is an inherent property of real-world time series, leading to varied distributions even within a short context window of a single time series. Frequency-level specialization is too coarse-grained to capture this level of diversity. To address these limitations, this paper introduces MOIRAI-MOE, using a single input/output projection layer while delegating the modeling of diverse time series patterns to the sparse mixture of experts (MoE) within Transformers. With these designs, MOIRAI-MOE reduces reliance on human-defined heuristics and enables automatic token-level specialization. Extensive experiments on 39 datasets demonstrate the superiority of MOIRAI-MOE over existing foundation models in both in-distribution and zero-shot scenarios. Furthermore, this study conducts comprehensive model analyses to explore the inner workings of time series MoE foundation models and provides valuable insights for future research.

1 INTRODUCTION

Foundation models have transformed several fields, such as natural language processing (Dubey et al., 2024) and computer vision (Kirillov et al., 2023), demonstrating impressive zero-shot performance. Inspired by these successes, time series forecasting is experiencing a similar shift (Liang et al., 2024). The traditional approach of developing separate models for each dataset is being replaced by the concept of universal forecasting (Woo et al., 2024), where a pretrained model can be applied across diverse downstream tasks in a zero-shot manner, regardless of variations in domain, frequency, dimensionality, context, or prediction length. This new paradigm significantly reduces the complexity of building numerous specialized models, paving the way for forecasting-as-a-service.

To excel in zero-shot forecasting, time series foundation models are pretrained on massive data from a variety of sources. However, unlike language and vision modalities which benefit from standardized input formats, time series data is inherently heterogeneous, posing significant challenges for *unified time series training*. Existing solutions such as TEMPO (Cao et al., 2024) and UniTime (Liu et al., 2024a) leverage language prompts to provide data identification information, thereby discerning the source of data and achieving model specialization at the dataset level. MOIRAI (Woo et al., 2024)

*Work done during internship/industrial PhD at Salesforce AI Research.

†Corresponding author. Email: chenghao.liu@salesforce.com

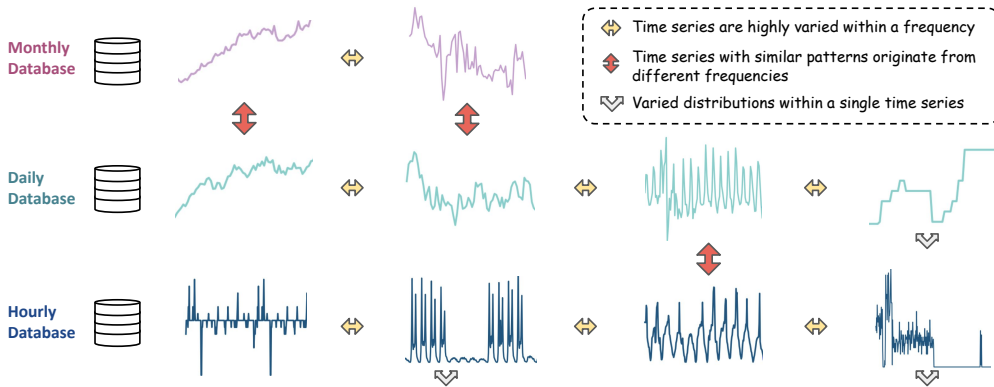


Figure 1: An illustration of the challenges arising from grouping time series by frequency and imposing frequency-level model specialization: the diversity of patterns within the same frequency group, the similarity of patterns across different frequencies, and the variability of distributions within a single time series. The examples presented are derived from **real time series** in the Monash benchmark (Godahewa et al., 2021).

goes a step further and proposes a more granular categorization based on a time series meta feature – frequency. Specifically, they design multiple input/output projection layers with each layer specialized to handle data corresponding to a specific frequency, thereby enabling frequency-level specialization. Similarly, TimesFM (Das et al., 2024) is also at this level of specialization, distinguishing the data by maintaining a frequency embedding mapping.

Given the heterogeneity of time series, we acknowledge the value of model specialization; however, we argue that *human-imposed frequency-level specialization lacks generalizability and introduces several limitations*. (1) Frequency is not always a reliable indicator and might not effectively capture the true structure of time series data. As shown in Figure 1, time series with different frequencies can exhibit similar patterns, while those with the same frequency may display diverse and unrelated patterns. This human-imposed mismatch between frequency and pattern undermines the efficacy of model specialization, resulting in inferior performance. (2) Furthermore, real-world time series are inherently non-stationary (Liu et al., 2022), displaying varied distributions even within a short context window of a single time series. Clearly, frequency-level specialization is too coarse-grained to capture this level of diversity, underscoring the need for more fine-grained modeling approaches.

To address the aforementioned issues, this paper introduces **MOIRAI-MOE**, an innovative solution for effective time series unified training, inspired by recent developments of Sparse Mixture of Experts (MoE) Transformers (Lepikhin et al., 2021; Fedus et al., 2022; Dai et al., 2024). The core idea of MOIRAI-MOE is to utilize a single input/output projection layer while delegating the modeling of diverse time series patterns to the sparse specialized experts in Transformer layers. With these designs, specialization of MOIRAI-MOE is achieved in a data-driven manner and operates at the token level. Moreover, this study investigates existing expert gating functions that generally use a randomly initialized linear layer for expert assignments (Shazeer et al., 2017; Jiang et al., 2024) and introduces a new function that leverages cluster centroids derived from a pretrained model to guide expert allocations.

We extensively evaluate MOIRAI-MOE using a total of 39 datasets in in-distribution and zero-shot forecasting scenarios. The results confirm the superiority of MOIRAI-MOE over state-of-the-art foundation models including TimesFM (Das et al., 2024), Chronos (Ansari et al., 2024), and MOIRAI (Woo et al., 2024). Additionally, we conduct comprehensive model analyses, as the first attempt, to explore the inner workings of time series MoE foundation models. It reveals that MOIRAI-MOE acquires the capability to achieve frequency-invariant representations and essentially performs progressive denoising throughout the model. Our contributions are summarized as follows:

- We propose MOIRAI-MOE, the first mixture-of-experts time series foundation models, achieving token-level model specialization in a data-driven manner. We introduce a new expert gating function for accurate expert assignments and improved performance.

- Extensive experiments on 39 datasets reveal that MOIRAI-MOE delivers up to 17% performance improvements over MOIRAI at the same level of model size, and outperforms other time series foundation models with up to $65\times$ fewer activated parameters.
- We conduct thorough model analyses to deepen understanding of the inner workings of time series MoE foundation models and summarize valuable insights for future research.

2 RELATED WORK

Foundation Models for Time Series Forecasting Time series foundation models (Liang et al., 2024) serve as versatile zero-shot forecasting tools. A key challenge in training these models is accommodating the high diversity of time series data, underscoring the possible need for designing specialization modules. Current approaches like TEMPO (Cao et al., 2024) and UniTime (Liu et al., 2024a) utilize language-based prompts to identify data sources, facilitating model specialization at the dataset level. MOIRAI (Woo et al., 2024) advances this by focusing on a time series meta feature – frequency. This method designs separate input/output projection layers for specific frequencies, allowing for frequency-specific specialization. Similarly, TimesFM (Das et al., 2024) operates at this level of specialization by incorporating a frequency embedding dictionary to differentiate data. Some methods, like Chronos (Ansari et al., 2024), Lag-LLaMA (Rasul et al., 2023), Moment (Goswami et al., 2024), and Timer (Liu et al., 2024c), do not incorporate any specialization modules. Instead, they utilize the same architecture for all time series data, which can potentially increase the learning complexity and demand a large number of parameters to memorize the diverse input patterns. In this work, we propose to achieve automatic token-level specialization by using sparse mixture of experts, where diverse time series tokens are processed by specialized experts, while similar tokens share parameter space, thereby reducing learning complexity.

Sparse Mixture of Experts Mixture of experts (MoE) has emerged as an effective method for significantly scaling up model capacity while minimizing computation overhead in Large Language Models (LLMs) (Fedus et al., 2022; Dai et al., 2024; Zhu et al., 2024). In this study, our motivation for using MoE is primarily centered on its capacity to enable token-level model specialization. A common approach for integrating MoE into Transformers involves replacing Feed-Forward Networks (FFNs) with MoE layers. An MoE layer consists of multiple expert networks and a gating function, where each expert shares the same structure as a standard FFN. The gating function is responsible for producing a gating vector that indicates the expert assignment. The assignment is usually sparse to maintain computational efficiency in the MoE layer, meaning that each token is generally processed by only one (Fedus et al., 2022) or two (Rajbhandari et al., 2022; Jiang et al., 2024) experts.

3 METHODOLOGY

In this section, we present MOIRAI-MOE, a mixture-of-experts time series foundation model built upon MOIRAI (Woo et al., 2024). Figure 2 presents a comparison. While MOIRAI-MOE inherits many of the strengths of MOIRAI, its major enhancement lies in: rather than using multi heuristic-defined input/output projection layers to model time series with different frequencies, MOIRAI-MOE utilizes a single input/output projection layer while delegating the task of capturing diverse time series patterns to the sparse mixture of experts in the Transformer. In addition, MOIRAI-MOE proposes a novel gating function that leverages knowledge from a pretrained model, and adopts a decoder-only training objective to improve training efficiency by enabling parallel learning of various context lengths in a single model update. We describe each model component in the following parts.

3.1 TIME SERIES TOKEN CONSTRUCTION

Patching techniques, first introduced in PatchTST (Nie et al., 2023), have become a prevalent method in many state-of-the-art time series models (Das et al., 2024; Liu et al., 2024a; Woo et al., 2024). By aggregating adjacent time series data into patches, this technique effectively captures local semantic information and significantly reduces computational overhead when processing long inputs. Given a time series with length S , we segment it into non-overlapping patches of size P , resulting in a sequence of patches $\mathbf{x} \in \mathbb{R}^{N \times P}$, where $N = \lceil \frac{S}{P} \rceil$.

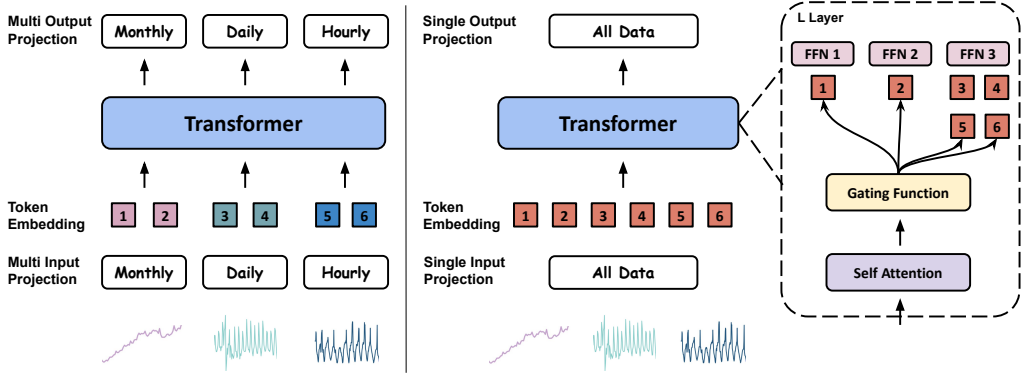


Figure 2: Comparison of MOIRAI (left) and MOIRAI-MOE (right).

We then normalize the patches to mitigate distribution shift issues (Liu et al., 2022; Wu et al., 2023). In a decoder-only (autoregressive) model, where each patch predicts its succeeding patch, applying a causal normalizer to each patch is the most effective way to achieve accurate normalization. However, this approach generates N subsequences with different lengths, diminishing the parallel training that decoder-only models typically offer. To address this, we introduce the masking ratio r as a hyperparameter, which specifies the portion of the entire sequence used exclusively for robust normalizer calculation, without contributing to the prediction loss.

Finally, we forward the patches through a single projection layer to generate time series tokens $x \in \mathbb{R}^{N \times D}$, where D is the dimension of the Transformers. And we pass on the capability of learning time series with diverse patterns to the vast number of parameters in the Transformer. This projection layer is implemented as a residual multi-layer perceptron to enhance representation capacity (Das et al., 2023).

3.2 MIXTURE OF EXPERTS FOR TRANSFORMERS

A decoder-only Transformer (Dubey et al., 2024) is constructed by stacking L layers of Transformer blocks, where each block can be represented as follows:

$$\tilde{x}^{l-1} = \text{CSA}(\text{LN}(x^{l-1})) + x^{l-1} \quad (1)$$

$$x^l = \text{FFN}(\text{LN}(\tilde{x}^{l-1})) + \tilde{x}^{l-1} \quad (2)$$

where CSA, FFN, and LN denote a causal self-attention module, a feed-forward network, and the layer normalization, respectively. Following MOIRAI (Woo et al., 2024), MOIRAI-MOE captures multivariate correlations by flattening all variates into a sequence. During causal attention, each token is allowed to attend to its preceding tokens, as well as preceding tokens from other variates.

Next, we establish the mixture of experts by replacing each FFN with a MoE layer, which is composed of M expert networks $\{E_1, \dots, E_M\}$ and a gating function G . Only a subset of experts is activated for each token, allowing experts to specialize in distinct patterns of time series data and ensuring computational efficiency. The output of the MoE layer is computed as:

$$\sum_{i=1}^M G(\tilde{x}^{l-1})_i \cdot E_i(\tilde{x}^{l-1}) \quad (3)$$

where $E_i(\tilde{x}^{l-1})$ is the output of the i -th expert network, and $G(\tilde{x}^{l-1})_i$ is the i -th token-to-expert affinity score generated by the gating function. Following Lepikhin et al. (2021); Rajbhandari et al. (2022); Jiang et al. (2024), we set the number of activated experts to $K = 2$.

3.2.1 GATING FUNCTION

Linear Projection as Gating Function. A popular and effective gating function takes the softmax over the TopK logits of a linear projection parameterized by $\mathbf{W}_g \in \mathbb{R}^{D \times M}$ (Shazeer et al., 2017;

Jiang et al., 2024; Dai et al., 2024):

$$G(\tilde{\mathbf{x}}^{l-1}) = \text{Softmax}(\text{TopK}(\tilde{\mathbf{x}}^{l-1} \cdot \mathbf{W}_g)) \quad (4)$$

However, the sparse gating can result in a load balancing issue (Shazeer et al., 2017). To mitigate this, an auxiliary loss is typically introduced to encourage an even distribution of tokens across experts (Lepikhin et al., 2021; Fedus et al., 2022; Jiang et al., 2024; Dai et al., 2024). Formally, the load balancing loss for a batch \mathcal{B} containing T tokens is defined as:

$$\mathcal{L}_{\text{load}} = M \sum_{i=1}^M \mathcal{D}_i \mathcal{P}_i, \text{ where } \mathcal{D}_i = \frac{1}{T} \sum_{\mathbf{x} \in \mathcal{B}} \mathbb{1}\{\text{argmax } G(\tilde{\mathbf{x}}^{l-1}) = i\}, \mathcal{P}_i = \frac{1}{T} \sum_{\mathbf{x} \in \mathcal{B}} G(\tilde{\mathbf{x}}^{l-1})_i \quad (5)$$

where \mathcal{D}_i denotes the fraction of tokens routed to expert i and \mathcal{P}_i indicates the proportion of the gating probability allocated to expert i .

Token Clusters as Gating Function. In this work, we propose a new gating mechanism that leverages cluster centroids derived from the token representations of a pretrained model to guide expert allocations. The intuition behind this approach is that clusters of pretrained token embeddings more closely reflect the real distribution of the data, leading to more effective expert specialization compared to a randomly initialized linear projection layer. Specifically, we utilize the self-attention output representations $\tilde{\mathbf{x}}^{l-1}$ of a pretrained model (in our case, we use the MOIRAI model) and apply k-means clustering to generate clusters. The number of clusters is set to match the total number of experts. During MoE training, each token computes the Euclidean distance to each cluster centroid $\mathbf{C} \in \mathbb{R}^{M \times D}$, and these distances serve as token-to-expert affinity scores for expert assignments:

$$G(\tilde{\mathbf{x}}^{l-1}) = \text{Softmax}(\text{TopK}(\text{Euclidean}(\tilde{\mathbf{x}}^{l-1}, \mathbf{C}))) \quad (6)$$

3.3 TRAINING OBJECTIVE

Let $\mathbf{x}_{t-l+1:t} = \{\mathbf{x}_{t-l+1}, \dots, \mathbf{x}_t\}$ denote the context window of length l for a token at position t . In this study, to facilitate both point and probabilistic forecasting, our goal is formulated as forecasting the predictive distribution of the next token $p(\mathbf{x}_{t+1}|\phi)$ by predicting the mixture distribution parameters $\hat{\phi}$ (Woo et al., 2024). These parameters are derived from the output tokens of the Transformer, followed by a single output projection layer. The following negative log-likelihood is minimized during training:

$$\mathcal{L}_{\text{pred}} = -\log p(\mathbf{x}_{t+1}|\hat{\phi}), \hat{\phi} = f_{\theta}(\mathbf{x}_{t-l+1:t}) \quad (7)$$

4 EXPERIMENTS

4.1 MOIRAI-MOE SETUP

To ensure a fair comparison with MOIRAI in terms of activated parameters, we configure the number of activated experts as $K = 2$ for MOIRAI-MOE, resulting in 11M/86M activated parameters per token for MOIRAI-MOE_S/MOIRAI-MOE_B, closely matching the dense model MOIRAI_S/MOIRAI_B that contains 14M/91M activated parameters. The total number of experts M is set to 32, yielding total parameter sizes of 117M for MOIRAI-MOE_S and 935M for MOIRAI-MOE_B. MOIRAI-MOE_L is not presented due to the significant requirements of computational resources. All MOIRAI-MOE models are trained on 16 A100 (40G) GPUs using a batch size of 1,024 and bfloat16 precision.

Table 1: Model configurations of MOIRAI and MOIRAI-MOE.

Model	Layers	d_{model}	d_{ff}	Activated Params	Total Params	Activated Experts	Total Experts
MOIRAI _S	6	384	1,024	14M	14M	–	–
MOIRAI _B	12	768	2,048	91M	91M	–	–
MOIRAI _L	24	1,024	2,736	310M	310M	–	–
MOIRAI-MOE _S	6	384	512	11M	117M	2	32
MOIRAI-MOE _B	12	768	1,024	86M	935M	2	32

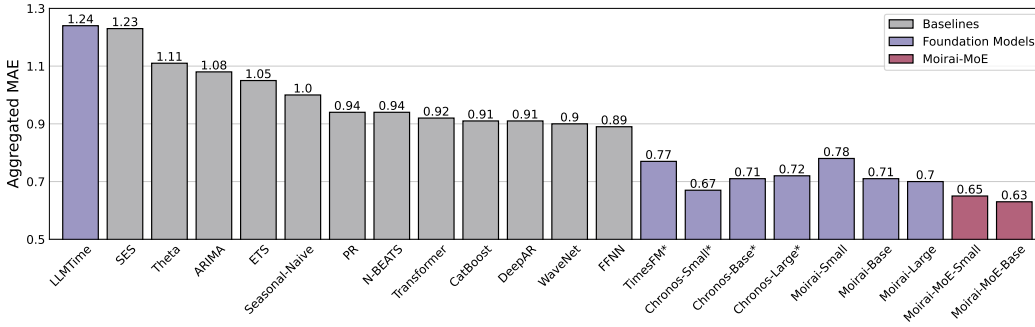


Figure 3: In-distribution forecasting evaluation using **29** datasets from Monash (Godaheewa et al., 2021). We use asterisks (*) to mark the methods that used the evaluation datasets here in their pretraining corpora. Aggregate MAE is reported, where the MAE for each dataset is normalized by the MAE of the seasonal naive forecast and the results are combined using the geometric mean.

Table 2: Zero-shot performance of probabilistic and point forecasting. We use asterisks (*) to mark the non-zero-shot datasets because they were used in the pretraining corpus of TimesFM and Chronos. The Average column is normalized by seasonal naive, followed by geometric mean. Best average results are highlighted in **red**, and second best results are in **blue**. Power: Turkey Power. Traffic: Istanbul Traffic. Weather: Jena Weather. BizITObs: BizITObs-L2C.

Method	Metric	Electricity	Solar	Power	ETT1	ETT2	Traffic	MDENSE	Walmart	Weather	BizITObs	Average
Seasonal Naive	CRPS	0.070	0.512	0.085	0.515	0.205	0.257	0.294	0.151	0.068	0.262	1.000
	MASE	0.881	1.203	0.906	1.778	1.390	1.137	1.669	1.236	0.782	0.986	1.000
TiDE	CRPS	0.048	0.420	0.046	1.056	0.130	0.110	0.091	0.077	0.054	0.124	0.631
	MASE	0.706	1.265	0.904	6.898	2.189	0.618	0.911	0.814	0.832	0.450	0.931
PatchTST	CRPS	0.052	0.518	0.054	0.304	0.131	0.112	0.070	0.082	0.059	0.074	0.549
	MASE	0.753	1.607	1.234	1.680	2.168	0.653	0.732	0.867	0.844	0.266	0.808
iTransformer	CRPS	0.057	0.443	0.056	0.344	0.129	0.105	0.072	0.070	0.053	0.077	0.540
	MASE	0.875	1.342	1.076	2.393	1.841	0.581	0.727	0.761	0.623	0.271	0.767
TimesFM	CRPS	0.045*	0.456	0.037	0.280	0.113	0.131	0.070	0.067	0.042	0.080	0.488
	MASE	0.655*	1.391	0.851	1.700	1.644	0.678	0.702	0.735	0.440	0.310	0.689
Chronos _S	CRPS	0.043*	0.389*	0.038	0.360	0.097	0.124	0.087	0.079	0.089	0.087	0.543
	MASE	0.629*	1.193*	0.717	1.799	1.431	0.622	0.834	0.849	0.606	0.301	0.694
Chronos _B	CRPS	0.041*	0.341*	0.039	0.387	0.092	0.109	0.075	0.080	0.058	0.084	0.499
	MASE	0.617*	1.002*	0.722	1.898	1.265	0.553	0.712	0.849	0.583	0.301	0.656
Chronos _L	CRPS	0.041*	0.339*	0.038	0.404	0.091	0.117	0.075	0.073	0.062	0.084	0.500
	MASE	0.615*	0.987*	0.702	1.959	1.270	0.597	0.724	0.788	0.601	0.310	0.660
MOIRAI _S	CRPS	0.072	0.471	0.048	0.275	0.101	0.173	0.084	0.103	0.049	0.081	0.578
	MASE	0.981	1.465	0.948	1.701	1.417	0.990	0.836	1.048	0.521	0.301	0.798
MOIRAI _B	CRPS	0.055	0.419	0.040	0.301	0.095	0.116	0.104	0.093	0.041	0.078	0.520
	MASE	0.792	1.292	0.888	1.736	1.314	0.644	1.101	0.964	0.487	0.291	0.736
MOIRAI _L	CRPS	0.050	0.406	0.036	0.286	0.094	0.112	0.095	0.098	0.051	0.079	0.514
	MASE	0.751	1.237	0.870	1.750	1.436	0.631	0.957	1.007	0.515	0.285	0.729
MOIRAI-MoE _S	CRPS	0.046	0.429	0.036	0.288	0.093	0.108	0.071	0.090	0.056	0.081	0.497
	MASE	0.719	1.222	0.737	1.750	1.248	0.563	0.746	0.927	0.476	0.298	0.670
MOIRAI-MoE _B	CRPS	0.041	0.382	0.034	0.296	0.091	0.100	0.071	0.088	0.057	0.079	0.478
	MASE	0.638	1.161	0.725	1.748	1.247	0.510	0.721	0.918	0.509	0.290	0.651

The small and base model are trained for 50,000 and 250,000 steps on LOTSA (Woo et al., 2024), respectively. The patch size P is set to 16 and the masking ratio r for decoder-only training is 0.3 (the corresponding experiments are provided in Appendix B). For optimization, we utilize the AdamW optimizer with $lr = 1e-3$, weight decay = $1e-1$, $\beta_1 = 0.9$, $\beta_2 = 0.98$. We also apply a learning rate scheduler with linear warmup for the first 10,000 steps, followed by cosine annealing. The specific configurations are outlined in Table 1.

4.2 MAIN RESULTS

In-distribution Forecasting. We begin with an in-distribution evaluation using a total of **29** datasets from the Monash benchmark (Godaheewa et al., 2021). Their training set are included in LOTSA (Woo et al., 2024), holding out the test set which we now use for assessments. Figure 3 summarizes

the results based on the aggregated mean absolute error (MAE), in comparison with the baselines presented in the Monash benchmark and the recently released foundation models: TimesFM (200M) (Das et al., 2024), Chronos family (Ansari et al., 2024): Chronos_S (46M), Chronos_B (200M), Chronos_L (710M), and MOIRAI family (Woo et al., 2024): MOIRAI_S (14M), MOIRAI_B (91M), MOIRAI_L (310M). Full results are provided in Appendix A. The evaluation results show that MOIRAI-MOE beats all competitors. In particular, MOIRAI-MOE_S drastically surpasses its dense counterpart MOIRAI_S by 17%, and also outperforms the larger models MOIRAI_B and MOIRAI_L by 8% and 7%, respectively. MOIRAI-MOE_B delivers a further 3% improvement over MOIRAI-MOE_S. Compared to the foundation model Chronos, which MOIRAI could not surpass, MOIRAI-MOE successfully bridges the gap and delivers superior results with up to 65× fewer activated parameters.

Zero-shot Forecasting. Next, we conduct an out-of-distribution evaluation on **10** datasets not included in LOTSA (see dataset details in Appendix A). To establish a comprehensive comparison, we report results for both probabilistic and point forecasting, using continuous ranked probability score (CRPS) and mean absolute scaled error (MASE) as evaluation metrics. For baselines, we compare against foundation models TimesFM, Chronos, and MOIRAI, as well as state-of-the-art full-shot models trained on individual datasets: TiDE (Das et al., 2023), PatchTST (Nie et al., 2023), and iTransformer (Liu et al., 2024b). The results are presented in Table 2. **MOIRAI-MOE_B achieves the best zero-shot performance, even outperforming TimesFM and Chronos, which include partial evaluation data in their pretraining corpora.** When compared to all sizes of MOIRAI, MOIRAI-MOE_S delivers a 3%–14% improvement in CRPS and an 8%–16% improvement in MASE. These improvements are remarkable, considering that MOIRAI-MOE_S has only 11M activated parameters – 28× fewer than MOIRAI_L.

Summary. Our extensive evaluation validates the effectiveness of MOIRAI-MOE’s overall model design, demonstrates the strong generalization ability of MOIRAI-MOE, and emphasizes the superiority of token-level specialization over frequency-level approaches (TimesFM, MOIRAI) and models without a specialization module (Chronos). MOIRAI-MOE also performs significantly better than the full-shot models trained separately on each dataset, highlighting the exceptional capabilities of the foundation model.

4.3 ABLATION STUDIES

Model Design. In the main results, we simultaneously enable the mixture of experts and switch the training objective from a masked encoder approach to a decoder-only approach. To ensure a more rigorous comparison, we conduct further experiments where only the learning objective is changed. Table 3 presents the Monash evaluation results using the small model, with the first and last rows representing MOIRAI_S and MOIRAI-MOE_S, respectively. This outcome suggests that altering the learning objective alone yields modest performance improvements, while the major gains stem from leveraging experts for automatic token-level specialization.

Table 3: Model variants performance on Monash.

Model Variant	Aggregated MAE
Multi Projection w/ Masked Encoder	0.78
Multi Projection w/ Decoder-Only	0.75
Single Projection & MoE w/ Decoder-Only	0.65

Training Objective. We adopt the decoder-only training objective for its superior training efficiency compared to the masked encoder approach. To illustrate this, we conduct experiments with varying training steps, as shown in Figure 4 (left). The results show that the decoder-only approach consistently outperforms the masked encoder at each evaluated step. Moreover, decoder-only training with 50k steps achieves comparable performance to masked encoder training with 100k steps, highlighting the substantial efficiency gains provided by the decoder-only training objective.

Gating Function. In Figure 4 (right), we vary the total number of experts and examine the impact of different gating functions on performance. Across all gating functions, performance consistently improves as the number of experts increases. Notably, our proposed token clustering method proves to be consistently superior to the other gating function variants across all expert configurations. This indicates that the clustering approach aligns more closely with the inherent distribution of time series

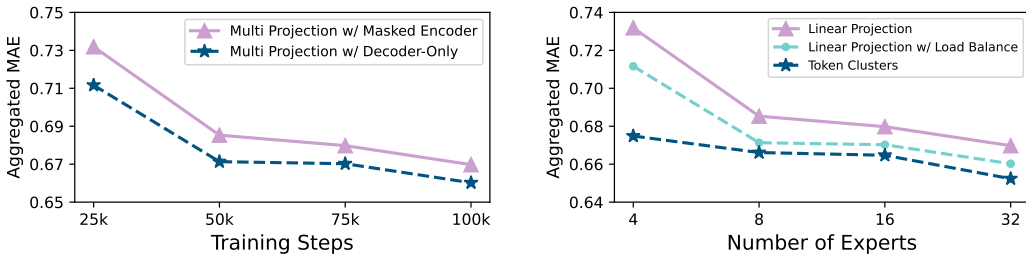


Figure 4: Ablation studies of the training objective and gating function using MOIRAI-MOE_S.

representations that have been optimized in pretraining, leading to more effective expert specialization compared to randomly learned-from-scratch gating. See more results in Appendix B.3.

4.4 MODEL ANALYSES

In this section, we delve deeper into the learned token embeddings and expert assignment distribution of MOIRAI-MOE to shed light on the inner workings of the time series MoE foundation model.

Obs 1: MOIRAI-MOE produces token embeddings in a data-driven way, effectively improving performance. In Figure 5, we utilize the T-SNE visualization tool (Van der Maaten & Hinton, 2008) to compare the token embeddings generated from the input projection layers of MOIRAI and MOIRAI-MOE. (1) In the first row, we examine the NN5 Daily and Traffic Hourly datasets, which have different frequencies but exhibit similar underlying patterns (visualizations of these patterns can be found in Appendix C). The figure illustrates that MOIRAI produces distinct embeddings due to the use of separate frequency projection layers, while MOIRAI-MOE successfully blends their representations together. Their inherent similarities are further demonstrated by their comparable expert allocation distributions in the last two columns. (2) In the second row, we analyze another daily frequency dataset, Covid Daily Deaths, which shows distinct patterns compared to NN5 Daily. We observe that the embeddings of these two datasets overlap to some extent in the MOIRAI model but are effectively separated in MOIRAI-MOE. Furthermore, the Covid Daily dataset shows different expert selection choices than NN5 Daily due to different token embeddings. **The data-driven modeling paradigm of MOIRAI-MOE ultimately leads to significant performance boosts**, reducing the MAE of NN5 Daily from 5.37 to 4.04 (a 25% improvement), the MAE of Traffic Hourly from 0.02 to 0.013 (a 35% improvement), and the MAE of Covid Daily Deaths from 124.32 to 119 (a 4% improvement).

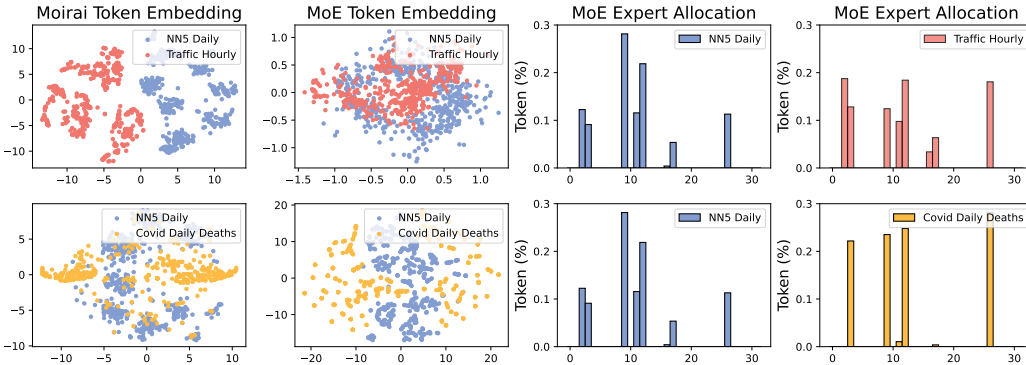


Figure 5: The first two columns are the comparison of embeddings from MOIRAI_S and MOIRAI-MOE_S. The last two columns are the expert assignment distributions of MOIRAI-MOE_S in layer 1: the x-axis corresponds to the 32 experts in a layer, and the y-axis is the proportion of tokens that choose experts.

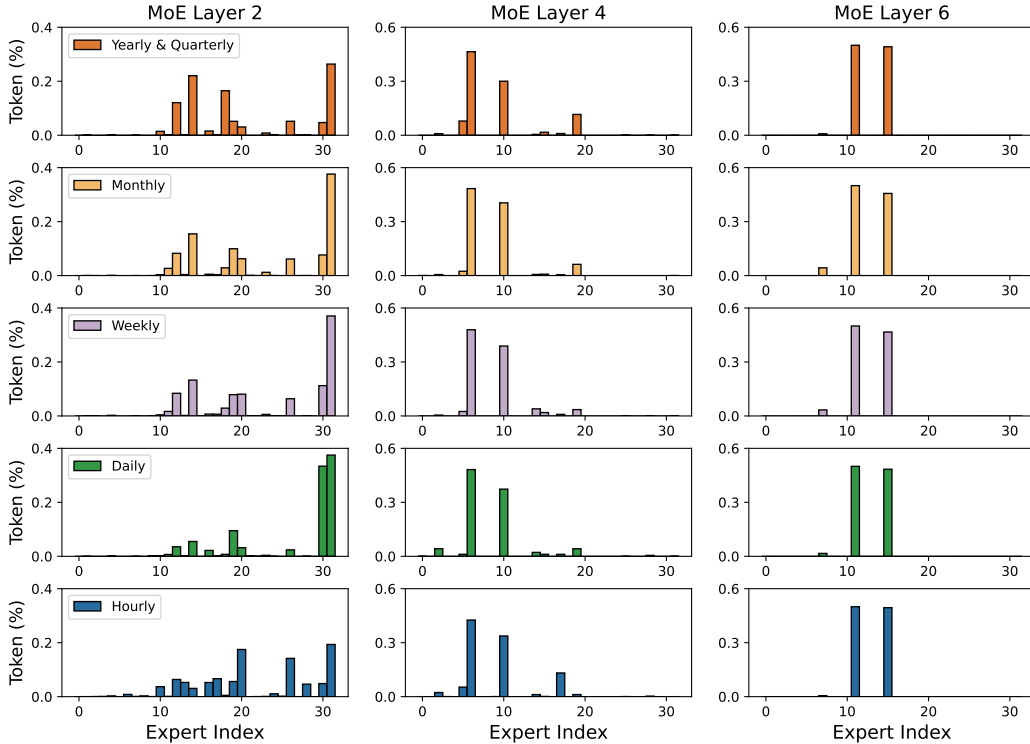


Figure 6: Visualization of the distribution of expert allocation for MOIRAI-MOE_S layers 2, 4, and 6 (the last layer) using the Monash benchmark grouped by time series frequency.

Obs 2: Different frequency data exhibit different expert selection distributions at shallow layers but similar distributions at deep layers. We present the expert allocation distributions on the Monash benchmark grouped by frequency in Figure 6. In the shallow layers, expert selection is notably diverse, indicating that the model relies on multiple experts to manage the high level of short-term variability, such as cyclical, seasonal, or abrupt changes. As tokens are aggregated in deeper layers, the model shifts its focus to more generalizable temporal dependencies, such as broader trends and long-term patterns, that can be shared across different frequencies and leads to more concentrated experts being selected. By the final layer (layer 6), expert allocation becomes nearly identical across all frequencies, suggesting that the model has abstracted time series into high-level representations largely independent of the frequency. This evidence indicates that **MOIRAI-MOE effectively achieves frequency-invariant hidden representations**, which are crucial for model generalization (Van Ness et al., 2023). The shared parameter space in the last layer also shows that it is sufficient for generating representations needed to make diverse predictions.

Obs 3: Shallow layers have more routing preferences than deep layers. According to Figure 6, as the layer index increases, expert selection gradually converges, with only 3 out of 32 experts being chosen by the final layer. This behavior contrasts with patterns observed in LLMs (Zhu et al., 2024), where earlier layers typically concentrate on a limited number of experts to capture common linguistic features, while deeper layers target more task-specific characteristics. This divergence may stem from the dynamic and noisier nature of time series tokens, which are generated from small time windows, unlike language tokens derived from a fixed vocabulary. **Our findings suggest that denoising processes occur progressively throughout the model.** This observation aligns with conclusions from GPT4TS (Zhou et al., 2023), which found that as the layer depth increases, token vectors are projected into the low-dimensional top eigenvector space of input patterns. Additionally, we recognize that some experts in MOIRAI-MOE are rarely selected. Pruning these underutilized experts for model compression is left for future work.

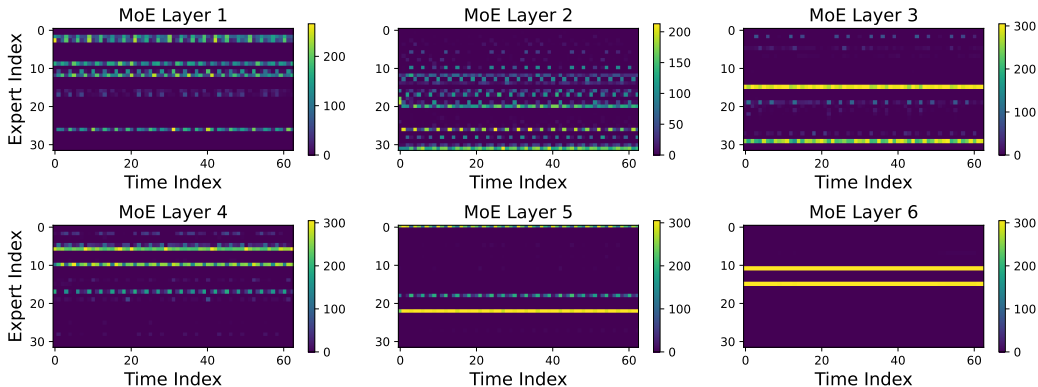


Figure 7: Visualization of expert allocation distributions for MOIRAI-MOE_S. All MoE layers are presented. The x-axis is the time index of the 63 time series tokens, generated from 1,000 context lengths. The y-axis corresponds to the 32 experts in a layer.

Obs 4: Expert allocation reflects time series periodicity patterns. To investigate the relationship between expert allocation and the positions of time series tokens, we use hourly data from the Monash repository with a minimum context length of 1,000 (e.g., the Traffic Hourly dataset). Figure 7 visualizes the expert choices at each token position. In the shallow layers, we observe that expert selection follows periodic patterns, consistent with the actual patterns in the raw data, as shown in Figure 11. This suggests that the model dynamically adapts to the cyclical nature of the traffic data, assigning specialized experts to manage tokens corresponding to distinct phases of the cycle, such as rising, peaks, and falling. In conclusion, **MOIRAI-MOE effectively learns to exploit time-based structures and the model specialization operates at the token level.**

4.5 EFFICIENCY ANALYSES

In this section, we aim to validate whether the inference speeds of MOIRAI and MOIRAI-MOE are comparable, as we have configured them with similar activated parameters. Additionally, due to the difference in the inference algorithms (the mask encoder in MOIRAI predicts all tokens simultaneously, while the decoder-only approach in MOIRAI-MOE generates predictions autoregressively), we evaluate the inference cost on a subset of the Monash benchmark where the predicted token is one (corresponding to 16 time steps) to eliminate this discrepancy. To also compare to the foundation model Chronos, we set the context length to 512 and the number of sampling samples to 20, aligning with the settings used in Chronos.

We present the summarized results in Table 4 and conclude that MOIRAI-MOE_S and MOIRAI-MOE_B exhibit similar inference times to MOIRAI_S and MOIRAI_B, respectively. These results highlight that MOIRAI-MOE not only maintains the same level of efficiency as MOIRAI but also delivers substantial performance improvements. Additionally, when comparing MOIRAI-MOE to Chronos, which also employs autoregressive inference algorithms, we find that MOIRAI-MOE is significantly faster. This speed advantage stems from the fact that MOIRAI-MOE generates predictions using patches of size 16, while Chronos can be viewed as using a patch size of 1, which greatly affects its inference efficiency.

Table 4: Inference cost evaluation. The values in brackets represent the parameter sizes of the foundation models. For MoE models, the two values indicate the number of activated parameters and the total number of parameters. The spent time is in seconds.

Model	Chronos _S (46M)	Chronos _B (200M)	Chronos _L (710M)	MOIRAI _S (14M)	MOIRAI _B (91M)	MOIRAI _L (310M)	MOIRAI-MOE _S (11M/117M)	MOIRAI-MOE _B (86M/935M)
Spent Time (s)	551	1,177	2,780	264	358	537	273	370

5 CONCLUSION

In this work, we introduce the first time series MoE foundation model MOIRAI-MOE that utilizes sparse experts to model diverse time series patterns in a data-driven manner. Empirical experiments demonstrate that, by enabling automatic token-level specialization, MOIRAI-MOE not only achieves significant performance improvements over all sizes of its predecessor MOIRAI, but also outperforms other competitive foundation models like TimesFM and Chronos with much fewer activated parameters. Moreover, we conduct comprehensive model analyses to gain a deeper understanding of time series MoE foundation models.

REFERENCES

- Abdul Fatir Ansari, Lorenzo Stella, Caner Turkmen, Xiyuan Zhang, Pedro Mercado, Huibin Shen, Oleksandr Shchur, Syama Sundar Rangapuram, Sebastian Pineda Arango, Shubham Kapoor, et al. Chronos: Learning the language of time series. *arXiv preprint arXiv:2403.07815*, 2024.
- Defu Cao, Furong Jia, Sercan O Arik, Tomas Pfister, Yixiang Zheng, Wen Ye, and Yan Liu. Tempo: Prompt-based generative pre-trained transformer for time series forecasting. In *International Conference on Learning Representations*, 2024.
- Damai Dai, Chengqi Deng, Chenggang Zhao, RX Xu, Huazuo Gao, Deli Chen, Jiashi Li, Wangding Zeng, Xingkai Yu, Y Wu, et al. Deepseekmoe: Towards ultimate expert specialization in mixture-of-experts language models. In *Association for Computational Linguistics*, 2024.
- Abhimanyu Das, Weihao Kong, Andrew Leach, Shaan Mathur, Rajat Sen, and Rose Yu. Long-term forecasting with tide: Time-series dense encoder. *Transactions on Machine Learning Research*, 2023.
- Abhimanyu Das, Weihao Kong, Rajat Sen, and Yichen Zhou. A decoder-only foundation model for time-series forecasting. In *International Conference on Machine Learning*, 2024.
- Abhimanyu Dubey, Abhinav Jauhri, Abhinav Pandey, Abhishek Kadian, Ahmad Al-Dahle, Aiesha Letman, Akhil Mathur, Alan Schelten, Amy Yang, Angela Fan, et al. The llama 3 herd of models. *arXiv preprint arXiv:2407.21783*, 2024.
- William Fedus, Barret Zoph, and Noam Shazeer. Switch transformers: Scaling to trillion parameter models with simple and efficient sparsity. *Journal of Machine Learning Research*, pp. 1–39, 2022.
- Rakshitha Godahewa, Christoph Bergmeir, Geoffrey I Webb, Rob J Hyndman, and Pablo Montero-Manso. Monash time series forecasting archive. *arXiv preprint arXiv:2105.06643*, 2021.
- Mononito Goswami, Konrad Szafer, Arjun Choudhry, Yifu Cai, Shuo Li, and Artur Dubrawski. Moment: A family of open time-series foundation models. *arXiv preprint arXiv:2402.03885*, 2024.
- Nate Gruver, Marc Finzi, Shikai Qiu, and Andrew G Wilson. Large language models are zero-shot time series forecasters. In *Advances in Neural Information Processing Systems*, 2023.
- Albert Q Jiang, Alexandre Sablayrolles, Antoine Roux, Arthur Mensch, Blanche Savary, Chris Bamford, Devendra Singh Chaplot, Diego de las Casas, Emma Bou Hanna, Florian Bressand, et al. Mixtral of experts. *arXiv preprint arXiv:2401.04088*, 2024.
- Jiawei Jiang, Chengkai Han, Wenjun Jiang, Wayne Xin Zhao, and Jingyuan Wang. Towards efficient and comprehensive urban spatial-temporal prediction: A unified library and performance benchmark. *arXiv e-prints*, pp. arXiv–2304, 2023.
- Alexander Kirillov, Eric Mintun, Nikhila Ravi, Hanzi Mao, Chloe Rolland, Laura Gustafson, Tete Xiao, Spencer Whitehead, Alexander C Berg, Wan-Yen Lo, et al. Segment anything. In *Proceedings of the IEEE/CVF International Conference on Computer Vision*, pp. 4015–4026, 2023.
- Guokun Lai, Wei-Cheng Chang, Yiming Yang, and Hanxiao Liu. Modeling long-and short-term temporal patterns with deep neural networks. In *The 41st international ACM SIGIR conference on research & development in information retrieval*, pp. 95–104, 2018.

- Dmitry Lepikhin, HyoukJoong Lee, Yuanzhong Xu, Dehao Chen, Orhan Firat, Yanping Huang, Maxim Krikun, Noam Shazeer, and Zhifeng Chen. Gshard: Scaling giant models with conditional computation and automatic sharding. In *International Conference on Learning Representations*, 2021.
- Yuxuan Liang, Haomin Wen, Yuqi Nie, Yushan Jiang, Ming Jin, Dongjin Song, Shirui Pan, and Qingsong Wen. Foundation models for time series analysis: A tutorial and survey. In *Proceedings of the 30th ACM SIGKDD Conference on Knowledge Discovery and Data Mining*, pp. 6555–6565, 2024.
- Xu Liu, Junfeng Hu, Yuan Li, Shizhe Diao, Yuxuan Liang, Bryan Hooi, and Roger Zimmermann. Unitime: A language-empowered unified model for cross-domain time series forecasting. In *Proceedings of the ACM on Web Conference 2024*, pp. 4095–4106, 2024a.
- Yong Liu, Haixu Wu, Jianmin Wang, and Mingsheng Long. Non-stationary transformers: Exploring the stationarity in time series forecasting. In *Advances in Neural Information Processing Systems*, pp. 9881–9893, 2022.
- Yong Liu, Tengge Hu, Haoran Zhang, Haixu Wu, Shiyu Wang, Lintao Ma, and Mingsheng Long. itransformer: Inverted transformers are effective for time series forecasting. In *International Conference on Learning Representations*, 2024b.
- Yong Liu, Haoran Zhang, Chenyu Li, Xiangdong Huang, Jianmin Wang, and Mingsheng Long. Timer: Generative pre-trained transformers are large time series models. In *Forty-first International Conference on Machine Learning*, 2024c.
- Yuqi Nie, Nam H Nguyen, Phanwadee Sinthong, and Jayant Kalagnanam. A time series is worth 64 words: Long-term forecasting with transformers. In *International Conference on Learning Representations*, 2023.
- Santosh Palaskar, Vijay Ekambaram, Arindam Jati, Neelamadhav Gantayat, Avirup Saha, Seema Nagar, Nam H Nguyen, Pankaj Dayama, Renuka Sindhgatta, Prateeti Mohapatra, et al. Automixer for improved multivariate time-series forecasting on business and it observability data. In *Proceedings of the AAAI Conference on Artificial Intelligence*, pp. 22962–22968, 2024.
- Samyam Rajbhandari, Conglong Li, Zhewei Yao, Minjia Zhang, Reza Yazdani Aminabadi, Ammar Ahmad Awan, Jeff Rasley, and Yuxiong He. DeepSpeed-moe: Advancing mixture-of-experts inference and training to power next-generation ai scale. In *International Conference on Machine Learning*, pp. 18332–18346, 2022.
- Kashif Rasul, Arjun Ashok, Andrew Robert Williams, Arian Khorasani, George Adamopoulos, Rishika Bhagwatkar, Marin Biloš, Hena Ghonia, Nadhir Vincent Hassen, Anderson Schneider, et al. Lag-llama: Towards foundation models for time series forecasting. *arXiv preprint arXiv:2310.08278*, 2023.
- Noam Shazeer, Azalia Mirhoseini, Krzysztof Maziarz, Andy Davis, Quoc Le, Geoffrey Hinton, and Jeff Dean. Outrageously large neural networks: The sparsely-gated mixture-of-experts layer. In *International Conference on Learning Representations*, 2017.
- Artur Trindade. Electricityloadaddiagrams20112014. UCI Machine Learning Repository, 2015. DOI: <https://doi.org/10.24432/C58C86>.
- Laurens Van der Maaten and Geoffrey Hinton. Visualizing data using t-sne. *Journal of machine learning research*, 9(11), 2008.
- Mike Van Ness, Huibin Shen, Hao Wang, Xiaoyong Jin, Danielle C Maddix, and Karthick Gopalswamy. Cross-frequency time series meta-forecasting. *arXiv preprint arXiv:2302.02077*, 2023.
- Will Cukierski Walmart Competition Admin. Walmart recruiting - store sales forecasting, 2014.
- Gerald Woo, Chenghao Liu, Akshat Kumar, Caiming Xiong, Silvio Savarese, and Doyen Sahoo. Unified training of universal time series forecasting transformers. In *International Conference on Machine Learning*, 2024.

- Haixu Wu, Jiehui Xu, Jianmin Wang, and Mingsheng Long. Autoformer: Decomposition transformers with auto-correlation for long-term series forecasting. In *Advances in neural information processing systems*, pp. 22419–22430, 2021.
- Haixu Wu, Tengge Hu, Yong Liu, Hang Zhou, Jianmin Wang, and Mingsheng Long. Timesnet: Temporal 2d-variation modeling for general time series analysis. In *International Conference on Learning Representations*, 2023.
- Haoyi Zhou, Shanghang Zhang, Jieqi Peng, Shuai Zhang, Jianxin Li, Hui Xiong, and Wancai Zhang. Informer: Beyond efficient transformer for long sequence time-series forecasting. In *Proceedings of the AAAI conference on artificial intelligence*, pp. 11106–11115, 2021.
- Tian Zhou, Peisong Niu, Liang Sun, Rong Jin, et al. One fits all: Power general time series analysis by pretrained lm. In *Advances in neural information processing systems*, pp. 43322–43355, 2023.
- Tong Zhu, Xiaoye Qu, Daize Dong, Jiacheng Ruan, Jingqi Tong, Conghui He, and Yu Cheng. Llama-moe: Building mixture-of-experts from llama with continual pre-training. *arXiv preprint arXiv:2406.16554*, 2024.

A EXPERIMENTAL DETAILS

In-distribution Forecasting Datasets. Following MOIRAI (Woo et al., 2024), we perform evaluations on 29 datasets from the Monash benchmark (Godahewa et al., 2021), including M1 Monthly, M3 Monthly, M3 Other, M4 Monthly, M4 Weekly, M4 Daily, M4 Hourly, Tourism Quarterly, Tourism Monthly, CIF 2016, Australian Electricity Demand, Bitcoin, Pedestrian Counts, Vehicle Trips, KDD Cup 2018, Australia Weather, NN5 Daily, NN5 Weekly, Carparts, FRED-MD, Traffic Hourly, Traffic Weekly, Rideshare, Hospital, COVID Deaths, Temperature Rain, Sunspot, Saugeen River Flow, and US Births. The statistics of data are provided in Table 5, and the full results of time series foundation models are shown in Table 6.

Table 5: Summary of datasets used in the in-distribution forecasting evaluations.

Dataset	Domain	Frequency	Number of Series	Prediction Length
M1 Monthly	Econ/Fin	M	617	18
M3 Monthly	Econ/Fin	M	1,428	18
M3 Other	Econ/Fin	M	174	8
M4 Monthly	Econ/Fin	M	48,000	18
M4 Weekly	Econ/Fin	W	359	13
M4 Daily	Econ/Fin	D	4,227	14
M4 Hourly	Econ/Fin	H	414	48
Tourism Quarterly	Econ/Fin	Q	427	8
Tourism Monthly	Econ/Fin	M	366	24
CIF 2016	Econ/Fin	M	72	12
Aus. Elec. Demand	Energy	30T	5	336
Bitcoin	Econ/Fin	D	18	30
Pedestrian Counts	Transport	H	66	24
Vehicle Trips	Transport	D	329	30
KDD Cup 2018	Energy	H	270	168
Australia Weather	Nature	D	3,010	30
NN5 Daily	Econ/Fin	D	111	56
NN5 Weekly	Econ/Fin	W	111	8
Carparts	Sales	M	2,674	12
FRED-MD	Econ/Fin	M	107	12
Traffic Hourly	Transport	H	862	168
Traffic Weekly	Transport	W	862	8
Rideshare	Transport	H	2,304	168
Hospital	Healthcare	M	767	12
COVID Deaths	Healthcare	D	266	30
Temperature Rain	Nature	D	32,072	30
Sunspot	Nature	D	1	30
Saugeen River Flow	Nature	D	1	30
US Births	Healthcare	D	1	30

Table 6: Full MAE results of time series foundation models on the Monash Benchmark. The other baseline results can be found in (Woo et al., 2024).

Dataset	Seasonal Naive	LLMTime	TimesFM	MOIRAI _{Small}	MOIRAI _{Base}	MOIRAI _{Large}	Chronos _{Small}	Chronos _{Base}	Chronos _{Large}	MOIRAI-MoE _{Small}	MOIRAI-MoE _{Base}
M1 Monthly	2,011.96	2,562.84	1,673.60	2,082.26	2,068.63	1,983.18	1,797.78	1,637.68	1,627.11	1,992.49	1,811.94
M3 Monthly	788.95	877.97	653.57	713.41	658.17	664.03	644.38	622.27	619.79	646.07	617.31
M3 Other	375.13	300.30	207.23	263.54	198.62	202.41	196.59	191.80	205.93	185.89	179.92
M4 Monthly	700.24	728.27	580.20	597.60	592.09	584.36	592.85	598.46	584.78	569.25	544.08
M4 Weekly	347.99	518.44	285.89	339.76	328.08	301.52	264.56	252.26	248.89	302.65	278.37
M4 Daily	180.83	266.52	172.98	189.10	192.66	189.78	169.91	177.49	168.41	172.45	163.40
M4 Hourly	353.86	576.06	196.20	268.04	209.87	197.79	214.18	230.70	201.14	241.58	217.35
Tourism Quarterly	11,405.45	16,918.86	10,568.92	18,352.44	17,196.86	15,820.02	7,823.27	8,835.52	8,521.70	9,508.07	7,374.27
Tourism Monthly	1,980.21	5,608.61	2,422.01	3,569.85	2,862.06	2,688.55	2,465.10	2,358.67	2,140.73	2,523.66	2,268.31
CIF 2016	743,512.31	599,313.84	819,922.44	655,888.58	539,222.03	695,156.92	649,110.99	604,088.54	728,981.15	453,631.21	568,283.48
Aus. Elec. Demand	455.96	760.81	525.73	266.57	201.39	177.68	267.18	236.27	330.04	215.28	227.92
Bitcoin	7.78E+17	1.74E+18	7.78E+17	1.76E+18	1.62E+18	1.87E+18	2.34E+18	2.27E+18	1.88E+18	1.55E+18	1.90E+18
Pedestrian Counts	65.60	97.77	45.03	54.88	54.08	41.66	29.77	27.34	26.95	41.35	32.37
Vehicle Trips	32.48	31.48	21.93	24.46	23.17	21.85	19.38	19.25	19.19	21.62	21.65
KDD Cup 2018	47.09	42.72	40.86	39.81	38.66	39.09	38.60	42.36	38.83	40.21	40.86
Australia Weather	2.36	2.17	2.07	1.96	1.80	1.75	1.96	1.84	1.85	1.76	1.75
NN5 Daily	8.26	7.10	3.85	5.37	4.26	3.77	3.83	3.67	3.53	4.04	3.49
NN5 Weekly	16.71	15.76	15.09	15.07	16.42	15.30	15.03	15.12	15.09	15.74	15.29
Carparts	0.67	0.44	0.50	0.53	0.47	0.49	0.52	0.54	0.53	0.45	0.44
FRED-MD	5,385.53	2,804.64	2,237.63	2,568.48	2,679.29	2,792.55	938.46	1,036.67	863.99	1,651.76	2,273.61
Traffic Hourly	0.013	0.030	0.009	0.020	0.010	0.010	0.013	0.012	0.010	0.013	0.014
Traffic Weekly	1.19	1.15	1.06	1.17	1.14	1.13	1.14	1.12	1.12	1.13	1.14
Rideshare	1.60	6.28	1.36	1.35	1.39	1.29	1.27	1.33	1.30	1.26	1.26
Hospital	20.01	25.68	18.54	23.00	19.40	19.44	19.74	19.75	19.88	20.17	19.92
COVID Deaths	353.71	653.31	623.47	124.32	126.11	117.11	207.47	118.26	190.01	119.00	102.92
Temperature Rain	9.39	6.37	5.27	3.30	5.08	5.27	5.35	5.17	5.19	5.33	5.36
Sunspot	3.93	3.07	1.07	0.11	0.08	0.13	0.20	2.45	3.45	0.10	0.08
Saugeen River Flow	21.50	34.84	25.16	24.07	24.40	24.76	23.57	25.54	26.25	23.05	24.40
US Births	1,152.67	1,374.99	461.58	872.51	624.30	476.50	432.14	420.08	432.14	411.61	385.24

Zero-shot Forecasting Datasets. We conduct zero-shot evaluations on the datasets listed in Table 7, which cover five domains and span frequencies ranging from minute-level to weekly. We use a non-overlapping rolling window approach, where the stride equals the prediction length. The test set consists of the last $h * r$ time steps, where h is the forecast horizon and r is the number of rolling evaluation windows. The validation set is defined as the last forecast horizon before the test set, while the training set includes all preceding data.

Table 7: Summary of datasets used in the zero-shot forecasting evaluations.

Dataset	Domain	Frequency	Prediction Length	Rolling Evaluations
Electricity (Trindade, 2015)	Energy	H	24	7
Solar (Lai et al., 2018)	Energy	H	24	7
Turkey Power ¹	Energy	H	24	7
ETT1 (Zhou et al., 2021)	Energy	D	30	3
ETT2 (Zhou et al., 2021)	Energy	D	30	3
Istanbul Traffic ²	Transport	H	24	7
M-DENSE (Jiang et al., 2023)	Transport	D	30	3
Walmart (Walmart Competition Admin, 2014)	Sales	W	8	4
Jena Weather (Wu et al., 2021)	Nature	10T	144	7
BizITObs-L2C (Palaskar et al., 2024)	Web/CloudOps	5T	48	20

Methods. The following is a brief introduction to the models used in the evaluation process.

- TiDE (Das et al., 2023) encodes the historical data of a time series along with covariates using dense multi-layer perceptrons (MLPs). It then decodes the time series while incorporating future covariates, also utilizing dense MLPs for this process.
- PatchTST (Nie et al., 2023) employs Transformer encoders combined with patching and channel independence techniques to enhance the performance of time series forecasting.
- iTransformer (Liu et al., 2024b) treats independent time series as tokens to effectively capture multivariate correlations through self-attention.
- LLMTime (Gruver et al., 2023) is a method for time series forecasting that leverages Large Language Models by encoding numerical data as text and generating possible future values through text completions.
- TimesFM (Das et al., 2024) is a decoder-only time series foundation model that pretrained on a large corpus of time series data, including both real-world and synthetic datasets.
- Chronos (Ansari et al., 2024) is an encoder-decoder time series foundation model that uses quantization to convert real numbers into discrete tokens.
- MOIRAI (Woo et al., 2024) is a time series foundation model trained on the LOTSA dataset, which contains over 27 billion observations across nine diverse domains.
- MOIRAI-MOE is proposed in this study, which is capable of achieving automatic token-level specialization.

Table 8: Hyperparameter search values for TiDE, PatchTST, and iTransformer.

	Hyperparameter	Values
TiDE	hidden_dim	{64, 128, 256}
	num_encoder_layers	[2, 6]
	num_decoder_layers	[2, 6]
PatchTST	d_model	{64, 128, 256}
	num_encoder_layers	[2, 6]
iTransformer	d_model	{128, 256, 512}
	num_encoder_layers	[2, 4]

¹<https://www.kaggle.com/datasets/dharanikra/electrical-power-demand-in-turkey>

²<https://www.kaggle.com/datasets/leonardo00/istanbul-traffic-index>

Hyperparameter Search. For the three full-shot models used in zero-shot forecasting part, i.e., TiDE (Das et al., 2023), PatchTST (Nie et al., 2023), and iTransformer (Liu et al., 2024b), we conduct hyperparameter search based on the values specified in Table 8. In addition, we explore the learning rate in the range $[1e-6, 1e-3]$ on a log scale, and set the context length as $l = m * h$, where m is tuned in the range $[2, 20]$, and h is the prediction length. We implement a random search across these parameters over 15 training runs and report results based on the best validation CRPS.

B ADDITIONAL RESULTS

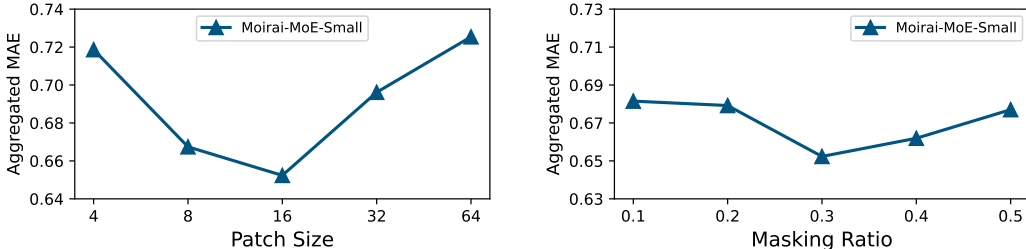


Figure 8: Effects of patch size and masking ratio using MOIRAI-MOE_S.

B.1 EFFECTS OF PATCH SIZE

In contrast to MOIRAI, which designs multiple input/output projection layers, each associated with a specific patch size, MOIRAI-MOE utilizes a single projection layer with a single patch size. In this part, we conduct experiments to examine the impact of different patch size choices. The evaluation results on the Monash benchmark are presented in Figure 8 (left), where the patch size of 16 yields the best performance. Increasing or decreasing this size results in performance degradation. Additionally, patch size affects inference speed; with a fixed context window, smaller patch sizes generate more time series tokens, increasing GPU memory usage and ultimately slowing down inference. For instance, using a patch size of 4 can take over a day to complete all evaluations. Our choice of a patch size of 16 not only delivers strong performance but also maintains a reasonable inference speed.

B.2 EFFECTS OF MASKING RATIO

In this study, we introduce the masking ratio r as a hyperparameter that determines the portion of the entire sequence used solely for robust normalizer calculation, helping to mitigate distribution shift issues. We conduct experiments to assess the effects of different masking ratios, with the evaluation results on the Monash benchmark shown in Figure 8 (right). A masking ratio of 0.3 delivers the best performance. A ratio of 0.1 uses too little data to compute a robust normalizer, potentially failing to accurately represent the overall sequence statistics. Conversely, a ratio of 0.5 masks half of the data, which may hinder the parallel learning efficiency in decoder-only training. Therefore, it is crucial to select an appropriate data range that is small enough to avoid excessive masking, yet sufficiently representative for robust normalizer computation.

B.3 EXPERT DISTRIBUTIONS OF DIFFERENT GATING FUNCTION

In this part, we present an in-depth comparison of the different gating functions explored in this study.

First, we provide additional details on the implementation of the proposed token clustering method. The core idea of this approach is to leverage cluster centroids derived from the token representations of a pretrained model to guide expert allocations. Specifically, we perform inference on our training corpus, LOTSA, using data amount corresponding to 100 epochs. During this process, we extract the self-attention output representations from a pretrained MOIRAI model and apply mini-batch k-means clustering to continuously update the clusters. The number of clusters is set to match the total number of experts. During the training of the MoE model, each token computes the Euclidean distance to each cluster centroid, and these distances are used as token-to-expert affinity scores for expert

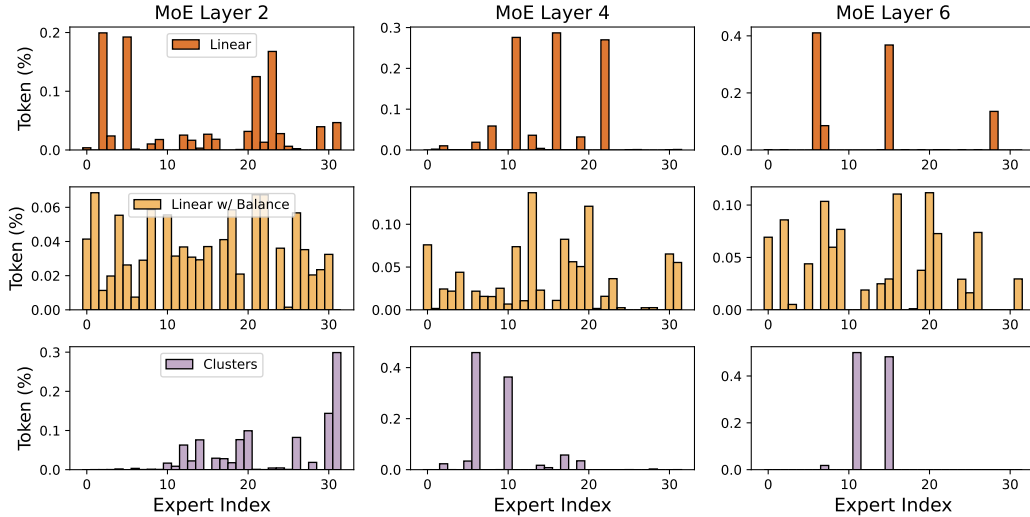


Figure 9: Visualization of the distribution of expert allocation for MOIRAI-MoE_S layers 2, 4, and 6 (the last layer) using all data from the Monash benchmark.

assignments. Empirical evaluations have demonstrated the effectiveness of this approach compared to randomly learned gating from scratch, indicating that the clustering method better aligns with the inherent distribution of time series representations.

Using the three gating functions explored in this study, i.e., linear projection, linear projection with load balancing, and token clustering, we present their expert allocation distributions aggregated across all datasets in the Monash benchmark, as illustrated in Figure 9. In terms of selection diversity, we observe the following relationships: Token Clusters (least diverse) < Pure Linear Projection (neutral) < Linear Projection with Load Balancing (most diverse). According to their performance results shown in Figure 4, we can establish the following ranking: Token Clusters > Linear Projection with Load Balancing > Pure Linear Projection. Based on all these observations, we offer the following explanation:

- In the token clusters approach, the expert selections are less diverse because the routing is grounded in pretrained knowledge. The clustering step creates centroids that represent well-structured patterns in the data, and then tokens are routed to specific experts that are particularly suited to handle the type of data represented by their corresponding cluster. While this targeted routing reduces diversity, it enhances performance due to the selection of experts based on more meaningful criteria.
- The addition of load balancing loss increases the diversity of expert selection by spreading the workload and encouraging the use of all experts more evenly. This diversity prevents over-reliance on specific experts, potentially improving generalization and performance compared to pure linear projection. However, this approach might be less targeted than clustering, since it still depends on a learned gating function rather than pretrained centroids.
- In the pure linear projection method, the gating function is entirely learned from scratch. Without any additional constraints (like load balancing), certain experts might get selected more often than others, leading to a neutral level of diversity. Since there is no mechanism to encourage exploration (like load balancing) or specialized routing (like clustering), performance remains lower than the other methods.

C VISUALIZATION

In this section, we visualize the datasets used in the model analyses (NN5 Daily (Figure 10), Traffic Hourly (Figure 11), and Covid Daily Deaths (Figure 12)) to facilitate understanding of the patterns within the time series data.

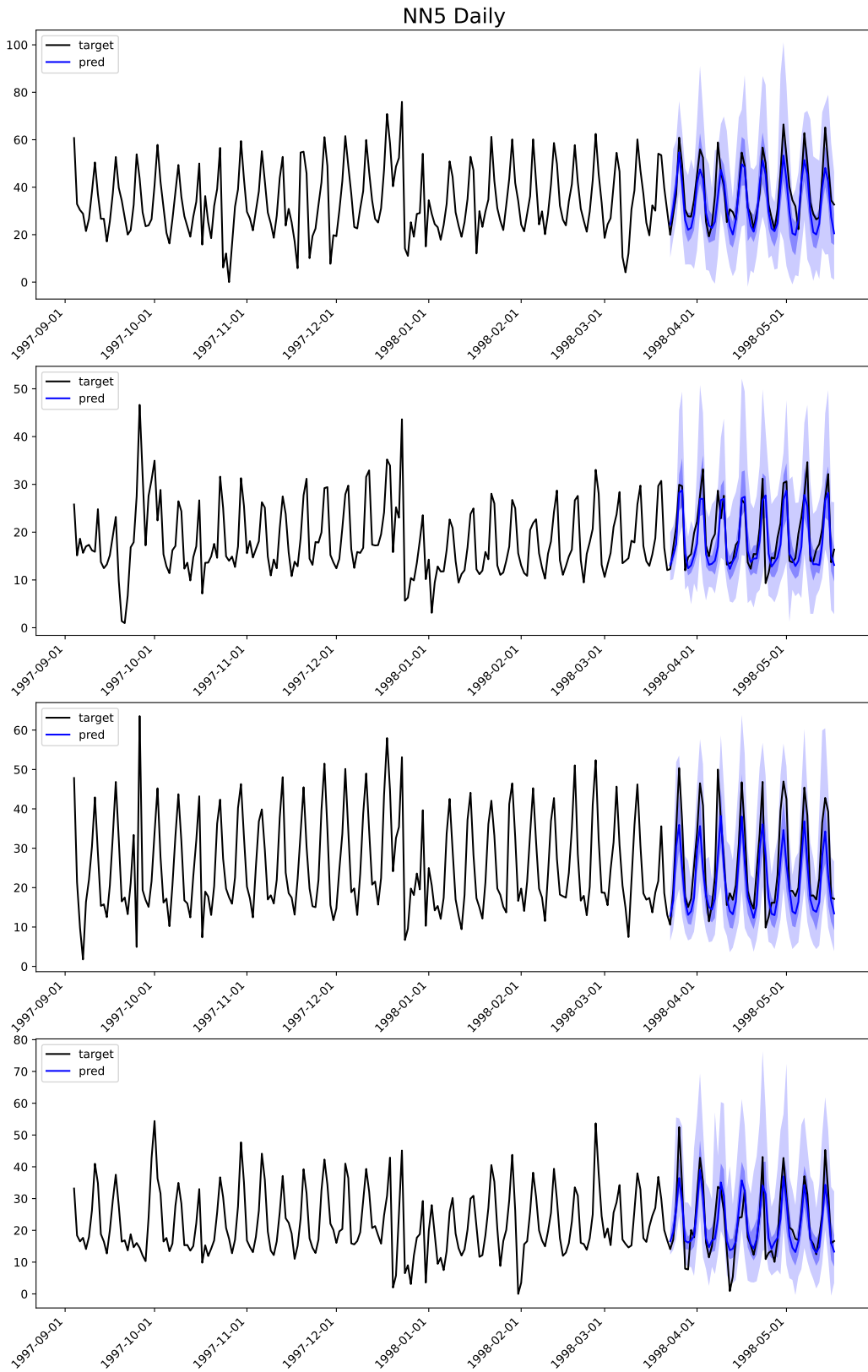


Figure 10: Visualization of NN5 Daily data, including both context length and forecast results.

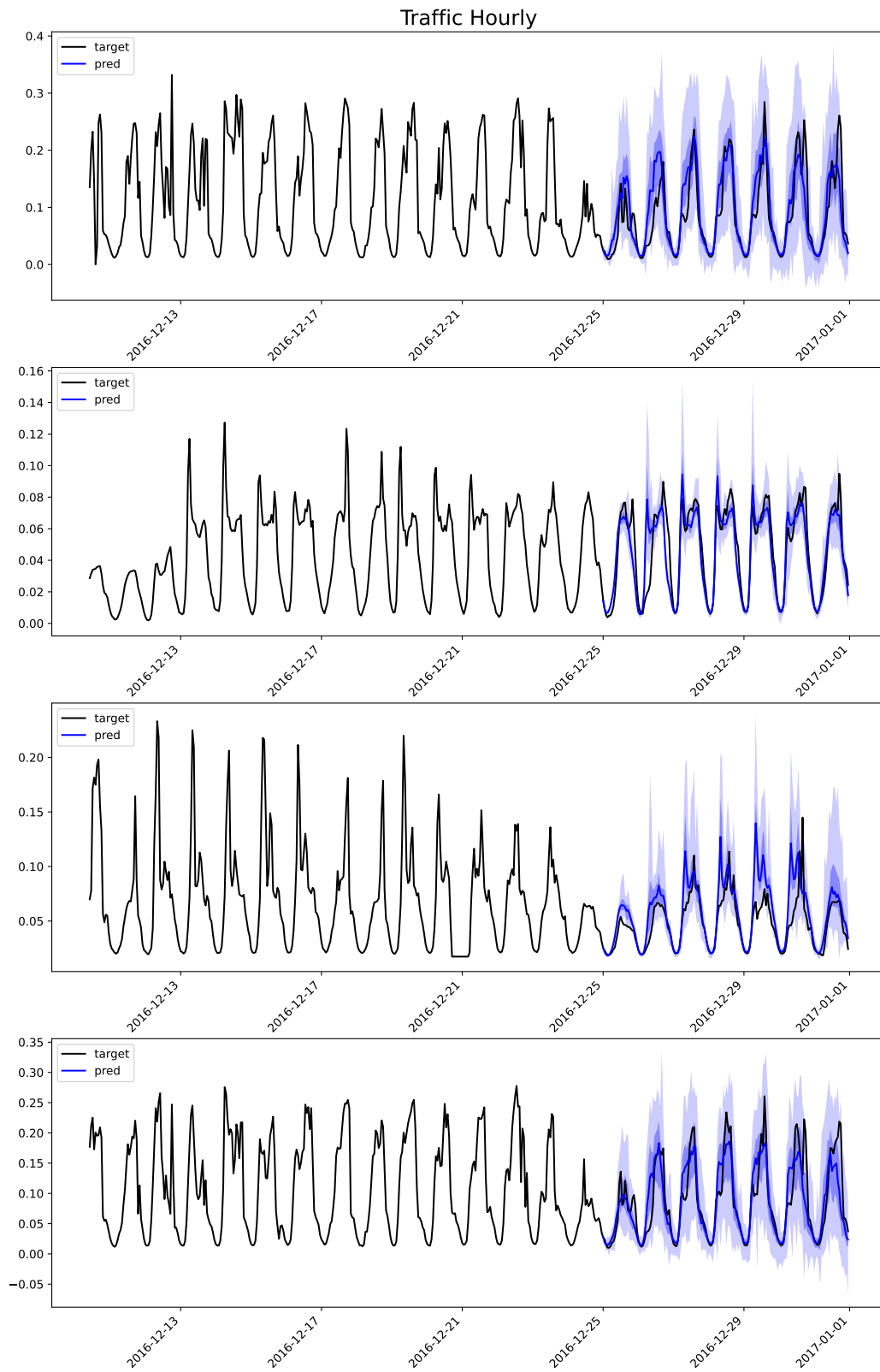


Figure 11: Visualization of Traffic Hourly data, including both context length and forecast results.

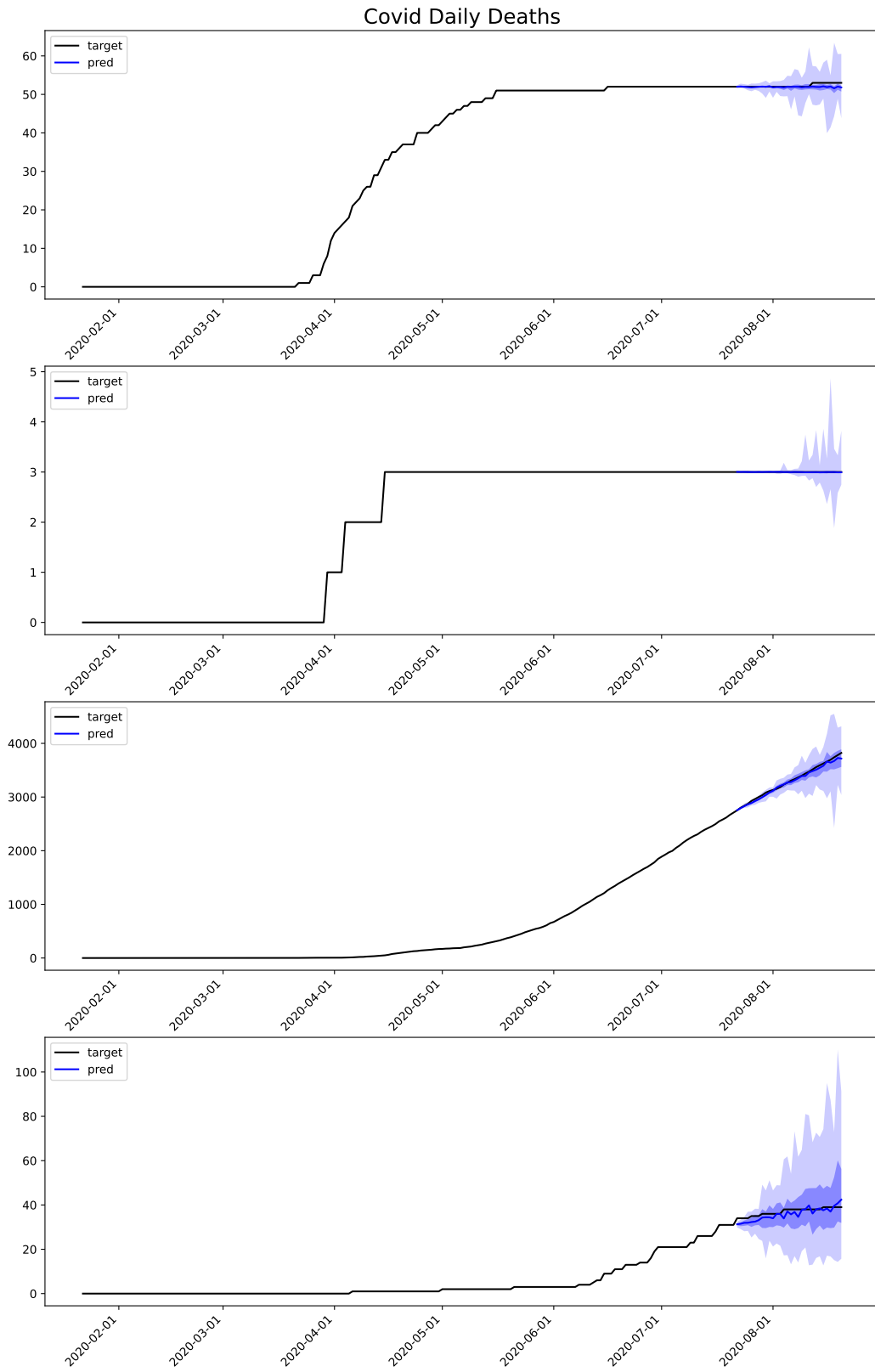


Figure 12: Visualization of Covid Daily Deaths, including both context length and forecast results.